IOP Publishing Measurement Science and Technology
Meas. Sci. Technol. **31** (2020) 054008 (11pp) https://doi.org/10.1088/1361-6501/ab6761

Echo-Lagrangian particle tracking: an ultrasound-based method for extracting path-dependent flow quantities

M D Jeronimo, M R Najjari and D E Rival

Department of Mechanical and Materials Engineering, Queen's University, Kingston, ON, Canada

E-mail: mark.jeronimo@queensu.ca

Received 1 November 2019, revised 20 December 2019
Accepted for publication 3 January 2020
Published 26 February 2020

Abstract

Eulerian, ultrasound-based velocimetry has become a popular tool for evaluating non-optically accessible flows, and has demonstrated great potential for medical flows. In contrast, the current study presents a Lagrangian method of extracting path-dependent dynamics from time-resolved ultrasound images referred to here as echo-Lagrangian particle tracking (echoLPT). Ultrasound system parameters specific to Lagrangian tracking are detailed for recording pulsatile flow through an idealized stenosis model. Furthermore, seeding materials and image processing procedures are discussed in order to improve signal-to-noise ratio and minimize particle image ambiguity. The pathlines that result from echoLPT reveal mixing downstream of the stenosis, and yield time-resolved, path-dependent information. As a means to demonstrate the value of echoLPT, particle residence time (PRT) in the post-stenotic region is calculated. PRT is the length of time a fluid parcel remains within a region of interest, and is used to highlight the effects of pulsatility. For the pulsatile flows tested, PRT is shown to increase with the frequency of pulsation as fluid is swept into the recirculation region, while PRT is decreased with increasing mean Reynolds number and amplitude ratio.

Keywords: Lagrangian particle tracking, particle residence time, ultrasound imaging, stenotic flow, pulsatile flow

S Supplementary material for this article is available online

(Some figures may appear in colour only in the online journal)

1. Introduction

In recent years, ultrasound imaging velocimetry (UIV), or echo-PIV, has been introduced and developed as a new tool for fluid dynamicists to study flows that are not optically accessible (Crapper *et al* 2000, Kim *et al* 2004, Leow and Tang 2018). The technique has drawn considerable interest from its ability to non-invasively measure *in vivo*, cardiovascular flows (Hong *et al* 2008, Zhang *et al* 2011). The ultrasound modality, also used by Doppler-based ultrasound velocity profiling (UVP), joins several other techniques, such as x-ray and magnetic resonance imaging (MRI), for opaque-flow velocimetry. UVP, reviewed in detail by Jensen *et al* (2016a, 2016b), is an Eulerian technique capable of producing results similar to UIV and has excellent temporal resolution, but requires a second transducer or signal modulation to yield two velocity components. MRI-based measurements boast a higher signal-to-noise ratio, compared to ultrasound, but have poor spatial and temporal resolution for velocimetry, and the cost can be inhibitive for many applications (Elkins and Alley 2007, van Ooij *et al* 2011). X-ray techniques are capable of Lagrangian particle tracking (LPT, or also known as PTV) but, in their current state, they are limited to slow acquisition rates (∼50 Hz) and very low Reynolds numbers ($Re < 1$), and must adhere to safety regulations for *in vivo* tests (Kertzscher *et al* 2004, Lee and Kim 2005, Im *et al* 2007). There have been a plethora of improvements to ultrasound-based velocimetry, as outlined by Poelma (2017), and including the recent incorporation of

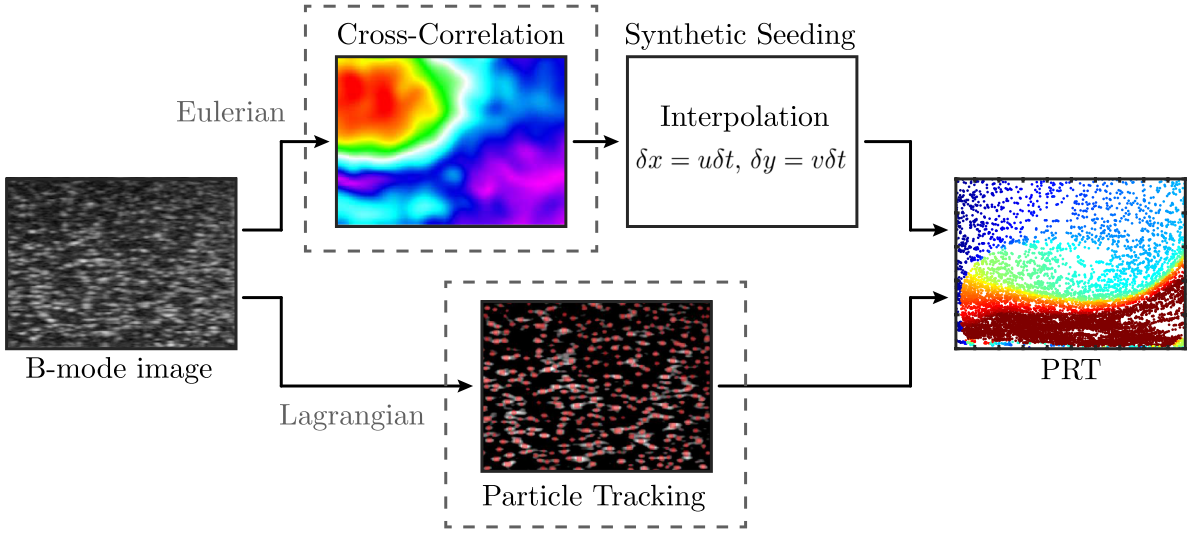

Figure 1. Path-dependent variables, like PRT, can be derived from both Eulerian and Lagrangian methods. The method described herein demonstrates how the more direct Lagrangian approach can be accomplished using ultrasound imaging.

particle tracking to improve Eulerian field measurements by Sampath *et al* (2018), but there is still no ultrasound-based LPT tool capable of extracting path-dependent flow quantities. Most recently, Ackermann and Schmitz (2016) as well as Song *et al* (2018) have developed an ultrasonic method for tracking the movement of an ultrasound contrast agent through *in vivo* microvessels. While their techniques reveal the position and velocity of microbubbles that can be used to describe the anatomy of the micro-vascular network, their movement is confined to minuscule channels on the order of 50 μm and a detailed reconstruction of the flow behaviour is not possible. In large-diameter vessels $\sim\mathcal{O}(10\ \text{mm})$, path-dependent (Lagrangian) hemodynamics are not clearly understood, especially in the presence of cardiovascular complications like stenoses and aneurysms, and thus require a direct-tracking approach to properly understand flow-derived risk factors.

Ultrasound-based particle tracking and path-dependent dynamics have many immediate applications over a broad range of fluid scales, including the study of multi-phase or sediment-laden flows, and understanding the intricacies of blood flow through diseased vessels. One such Lagrangian metric is particle residence time (PRT), which is defined as the length of time a fluid parcel remains within a region of interest, and is an indicator of mixing and recirculation. Jeronimo *et al* (2019a) presented a technique for measuring PRT using two-dimensional LPT, and demonstrated the value of PRT extraction for unsteady flows through an *in vitro* stenosis model. *In vivo*, elevated PRT has been linked to increased plaque deposition, which promotes atherosclerotic development, in large blood vessels that are accessible using ultrasound imaging (Tambasco and Steinman 2003). Figure 1 shows two approaches for measuring PRT from ultrasound images. Current UIV techniques (Eulerian) require the additional step of synthetically seeding the computed velocity field to map particle displacements and calculate PRT. A Lagrangian approach, however, provides a direct path to the same information, as introduced for ultrasound imaging by Jeronimo *et al* (2019b).

In the current study, a procedure coined echo-Lagrangian particle tracking (echoLPT) is described as a novel method to extract Lagrangian metrics from time-resolved ultrasound images. Careful consideration is given to optimizing ultrasound parameters and image preprocessing steps for accurate particle detection and tracking. To demonstrate the feasibility and value of echoLPT, PRT is measured within a post-stenotic recirculation region, and shown to reveal distinct differences based on the degree of pulsatility.

2. Methodology

2.1. Experimental setup

Experiments were performed in a table-top flow loop. A physiological piston pump (CompuFlow 1000, Shelley Medical Systems) drives flow laden with ultrasound contrast agent through an acrylic pipe with an inner diameter (D) of 22 mm and wall thickness of 1.6 mm. Approximately $100D$ downstream of the pipe entrance is a 3D-printed, idealized stenosis model consisting of a smooth contraction of the flow loop's internal pipe diameter, followed by a sudden expansion, as depicted in figure 2. The diametrical contraction of the stenosis wall follows the smooth sinusoidal curve given by y for $-0.5 \leqslant x/L < 0$:

$$y(x) = \frac{1}{2}\left[d + (D-d)\sin^2\left(\frac{\pi x}{2L}\right)\right], \tag{1}$$

where x is the distance along the pipe, $d = D/2$ is the diameter of the stenosis throat, and $L = 22$ mm is the length of the stenosis model. The stenosis geometry creates a recirculation region immediately downstream of the expansion, and is one of many poorly understood *in vivo* geometries that would be targeted for echo LPT analysis.

An ultrasound transducer acts as a transmitter and receiver of high frequency sound waves that are reflected at interfaces between mediums of different acoustic impedances. A 128-element linear-array transducer (BK Medical) was aligned with the

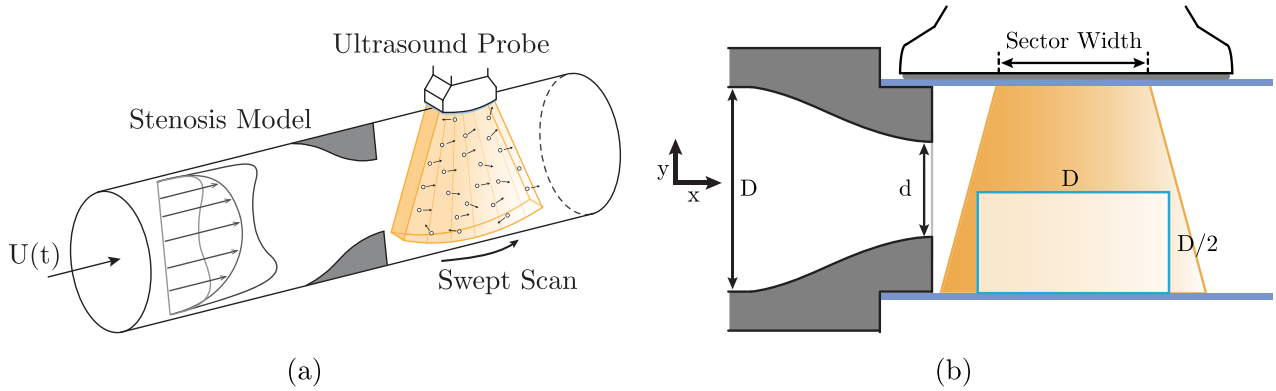

Figure 2. (a) Schematic of pulsatile flow, $U(t)$, through an axisymmetric stenosis model. A linear-array ultrasound transducer situated at the stenosis exit records the motion of microbubbles suspended in the fluid. (b) Cross-section of the stenosis and field-of-view. The sector width of the ultrasound beam is set to 50% to maximize the acquisition rate, but shifts the measurement domain (blue outline) away from the wall of stenosis. This figure is not to scale.

centreline of the pipe and affixed just downstream of the stenosis model. The test section, which includes the stenosis model and transducer head (depicted in figure 2(a)), is submerged in water to mitigate strong reflections caused by the acoustic impedance difference between the transducer and air. Care must be taken to choose materials for the test section that minimize reflections of the incident ultrasound signal. Acrylic and elastomeric materials (e.g. Sylgard-184) were each tested and have impedances similar to that of the working fluid, a glycerol-water solution. However, Sylgard-184 has a large attenuation coefficient and quickly attenuates the strength of acoustic signals, and was discarded in favour of acrylic. The strength of the transmitted signal is still substantially weakened using an acrylic flow loop—considerably so when compared to an equivalent optical setup—and there are bright reflection artifacts near the upper wall of the test section. As a result, the echoLPT measurement domain covers the bottom half of the pipe ($D/2$) and extends approximately one diameter (D) axially. In order to maximize the frame rate (discussed further in section 2.4), the sector width is reduced to 50%, which shifts the measurement domain away from the stenosis wall, as seen in figure 2(b).

2.2. Pulsatile flow conditions

The value of echo-Lagrangian particle tracking is highlighted by measuring the PRT of post-stenotic, pulsatile flows. The pulsatile flows tested are the sum of steady and oscillatory (sinusoidal) components. A mean Reynolds number (Re_m) defines the steady component, while the unsteady component is a function of the Womersley number ($\alpha = \frac{D}{2}\sqrt{2\pi f_p/\nu}$, where f_p is the frequency of pulsation and ν is the kinematic viscosity) and an amplitude ratio ($\lambda = (\mathrm{Re}_o - \mathrm{Re}_m)/\mathrm{Re}_m$, where Re_o is the peak Reynolds number of the oscillatory component). Three Reynolds numbers were compared ($\mathrm{Re}_m = 32$, 64 and 128), as well as two amplitudes ratios ($\lambda = 0.5$ and 1.0). At $\lambda = 1.0$, the flow rate is zero momentarily but never reverses. Two Womersley numbers ($\alpha = 15$ and 20) were chosen for their relevance to large artery blood flow. The working fluid, an aqueous solution with 40% w/w glycerol, has a kinematic viscosity, ν, of $3.4 \times 10^{-}6\ \mathrm{m}^2\ \mathrm{s}^{-1}$. The Re_m range is limited by the frame rate of the ultrasound transducer, but the recent development of plane-wave imaging could increase the acquisition rate into the kHz range (Leow *et al* 2015), and enable the investigation of high-Re turbulent flows (La Porta *et al* 2001). Nevertheless, the above flow conditions will serve to demonstrate how echoLPT can be used to extract Lagrangian particle sources and path-dependent quantities.

2.3. Seeding particles

To extract Lagrangian information from the post-stenotic flow it must be seeded with tracer particles that faithfully follow the flow and exhibit very high echogenicity (the ability to reflect incoming ultrasound waves). Traditionally, specially-designed ultrasound contrast agents are used for clinical ultrasound applications as well as in many, biomedically-inspired, UIV studies. However, seeding particles commonly used for PIV can also be used, as demonstrated by UIV using synthetic Nylon 12 particles (Gurung and Poelma 2016) and ultrasound speckle velocimetry using hollow glass spheres (Gallot *et al* 2013). In deciding on a tracer medium for echoLPT experiments, three particles were compared (as shown in figure 3): (a) polyamide particles, 20 μm; (b) hollow glass spheres, 9–13 μm; and (c) an ultrasound contrast agent, 1–10 μm. While the synthetic and glass particles effectively act as scatterers, the resultant images suffer from low signal-to-noise ratios and are unsuitable for Lagrangian tracking. In comparison, the contrast agent produces significantly less background noise and individual particle images can easily be discerned from one another. For the echoLPT measurements demonstrated in the current study, the ultrasound contrast agent, Definity microbubbles (Lantheus Medical Imaging), is used. The microbubbles are neutrally-buoyant, single micron-sized lipid-encapsulated perfluoropropane bubbles that have very high acoustic impedance and a Stokes number well below 1, and do not act as a dispersed phase within the single-phase working fluid. Definity has previously been used in UIV studies at similarly low Re_m *in vivo* and *in vitro* (Kheradvar *et al* 2010, Walker *et al* 2014).

In clinical applications, large volumes of contrast agent are used to effectively illuminate bulk blood flow, but the concentration must be carefully controlled for fluids research.

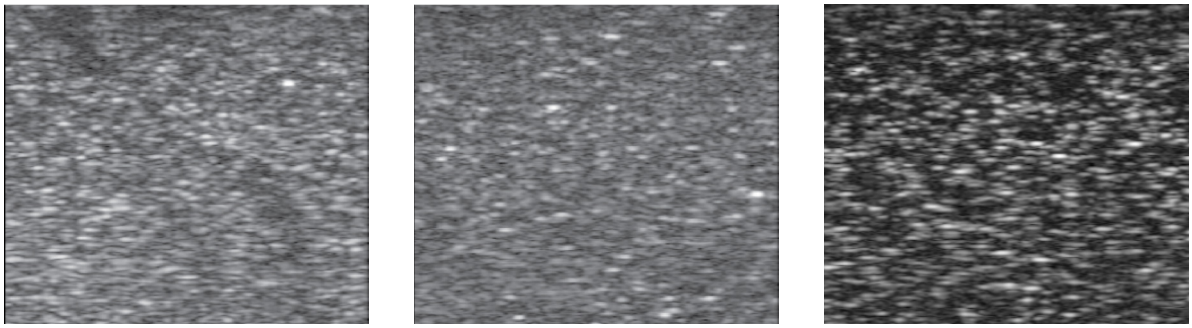

Figure 3. A comparison of B-mode images captured by seeding a quiescent fluid with (a) polyamide particles, (b) hollow glass spheres, and (c) an ultrasound contrast agent, Definity microbubbles. The contrast agent is specifically designed for ultrasound imaging and yields a higher signal-to-noise ratio and less particle ambiguity compared to the other seeding materials.

Table 1. EchoLPT ultrasound imaging parameters (for current setup).

Parameter	Description
Ultrasound system	SonixTouch Q +
Transducer	Linear L14-5/38, element pitch: 0.3 mm Frequency: 14 MHz
Beam line density	192
Acoustic power	33%
Gain	20%
Dynamic range	50%
Depth of scan	2.5 cm (range: 2–9 cm)
Depth of focus	1.7 cm
At focus:	
Axial resolution	0.3 mm
Lateral resolution	0.5 mm
Field of view	21.8 cm × 11.1 cm
Image acquisition rate	173 Hz
Maximum measured velocity	14.7 cm s^{-1}
Contrast agent	Definity microbubbles (Lantheus medical imaging), Bubble diameter: 1–10 μm
Ideal particle image density	0.005 particles per pixel (see figure 3(c))
Maximum particle image density	0.008 particles per pixel (see figure 6(a))

UIV studies have evaluated the effect of contrast agent concentration on velocimetry results and quote values in the range 800–2000 bubbles ml^{-1} for *in vitro* experiments (Kim *et al* 2004, Niu *et al* 2011). For the purpose of microbubble tracking, the concentration is reduced to approximately 500 bubbles ml^{-1}, or 250 bubbles in the measurement domain. The resultant detected particle image density is 0.005 particles per pixel (ppp). EchoLPT is highly sensitive to particle image density, much more so than UIV, due to its anisotropic, in-plane resolution. The axial resolution (along the beam) is constant, but the lateral resolution (along the direction of flow) is typically worse and deteriorates with distance from the focal point (the middle of the measurement domain in the current study). Primarily, the loss in resolution is caused by the spreading of the ultrasound beam and the resultant point spread function (PSF) of the contrast agent. A high concentration of microbubbles lowers the quality of particle detection by increasing particle image ambiguity—an issue that is exacerbated by the variability of the PSF, which distorts tracer images according to their distance from the focus (Contreras Ortiz *et al* 2012). The coupled effect jeopardizes particle detection and matching by producing densely-packed regions of blurry particle images that are difficult to discern from one and another. The chosen bubble concentration, within a narrow sector, ensures each bubble is identifiable and their shape does not change significantly between frames.

2.4. Contrast imaging parameters

A SonixTouch Q+ (BK Medical) ultrasound system is configured to maximize the frame rate and minimize particle ambiguity. The imaging parameters for the current experiment are discussed in detail here and summarized in table 1. Note that the values in table 1 should not be thought of as strict limits as they are specific to the experimental setup (e.g. pipe diameter). The frequency, line density and sector width of the emitted sound waves, and the gain and dynamic range of the received signal were all adjusted to optimize the brightness-mode (B-mode) images for echoLPT. At a frequency of 14 MHz, the gain and dynamic range of the system control image quality,

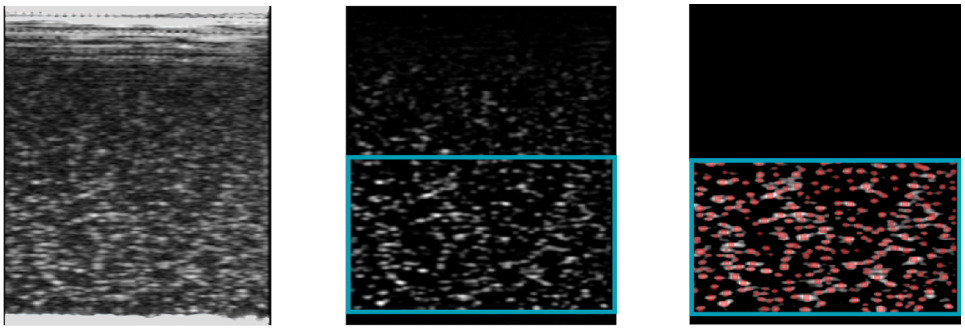

Figure 4. EchoLPT uses (a) low-seeding density B-mode images that are (b) preprocessed, using background and smoothing filters, to reduce particle image ambiguity and increase contrast. (c) Particles within the measurement domain are detected in each frame using peak detection. Detected particles are highlighted in red. The measurement domain is designated by a blue outline. (a) Raw B-mode image. (b) Preprocessed. (c) Detected particles.

where quality is judged by particle image shape and contrast, i.e. signal-to-noise ratio. For a given scan depth, the transducer's line density and sector width directly influence the frame rate. Here, a maximal frame rate of 173 Hz was achieved at a depth of 2.5 cm by setting the sector width to a minimum (50%) and the line density to 192 to retain good lateral resolution. The frame rate is a limiting factor on the flow conditions that can be investigated, and the Re_m and λ measured were chosen to constrain frame-to-frame bubble displacement to a maximum of 12 pixels. The ultrasound beam has a thickness of approximately 2 mm (10% of the diameter of the pipe) so this two-dimensional technique is actually operating on a volume. However, Jeronimo *et al* (2019a) showed that thick-sheet measurements can minimize particle loss due to out-of-plane motion without contributing significantly to tracking error.

The final B-mode image parameter that was adjusted was the acoustic power output of the ultrasound transducer. The power is a function of the frequency and pressure of the sound waves (often measured as a mechanical index, MI), and directly corresponds to the intensity of the reflected signal. While studying a similar geometry, Walker *et al* (2014) had difficulty observing microbubbles recirculating close to the wall and speculated that the bubbles did not follow the flow into those regions. In this study, we demonstrate how extended exposure to high acoustic power can rupture microbubbles. Video 1 (stacks.iop.org/MST/31/054008/mmedia) shows contrast microbubbles bursting as the acoustic power is quickly increased from low power to high. By reducing the power output, microbubbles could clearly be detected throughout the measurement domain. Also apparent in Video 1 is a downward motion of the contrast agent, in an otherwise quiescent fluid, when the power is increased. Flow is generated by acoustic forcing by the high power sound waves (typically referred to as acoustic streaming (Poelma 2017)) and affects all seeding particle types tested, as seen in Video 2 for hollow glass spheres. Rupture and acoustic streaming are avoided by recording at low acoustic power.

2.5. B-mode image preprocessing

Figure 4(a) shows an example of a B-mode image collected for echoLPT using the parameters discussed in section 2.4. The low particle image density and ease with which individual microbubbles can be identified are ideal for Lagrangian tracking. The aforementioned ultrasonic reflections near the top of the field of view are apparent and a smaller domain (outlined in blue in figure 4(b)) was selected for measurements. Despite the care that was taken while capturing the B-mode images, the signal-to-noise ratio is still relatively low and images must be thoroughly filtered before the detection and tracking processes. First, images are scaled using the sector width (50%), number of elements in the transducer (128) and horizontal pixel pitch of each element (0.3 mm) to compute the width of the field of view. Subtraction of the mean image intensity across all images removes stationary features, like reflection artifacts and noise, from the background of each frame. The images are then smoothed using a Gaussian smoothing filter, with a 9×9 pixel fit to account for large bubble images. The Gaussian filter rounds particles by smearing the peak intensity of each particle slightly. To refocus the particle images a sharpening filter is applied that reduces particle size once again to produce high contrast images. Figure 4(b) shows the result of the preprocessing steps. Due to the thickness of the measurement plane and noise inherent to the ultrasound modality, there is still considerable variability in the shape, size and intensity of particles. Each of these inconsistencies have been linked to errors in PIV measurements where they affect a particle image's contribution to the correlation function (Adrian and Westerweel 2011, Raffel *et al* 2018). Lagrangian tracking algorithms are not affected in this regard as they look for particle-specific matches from one

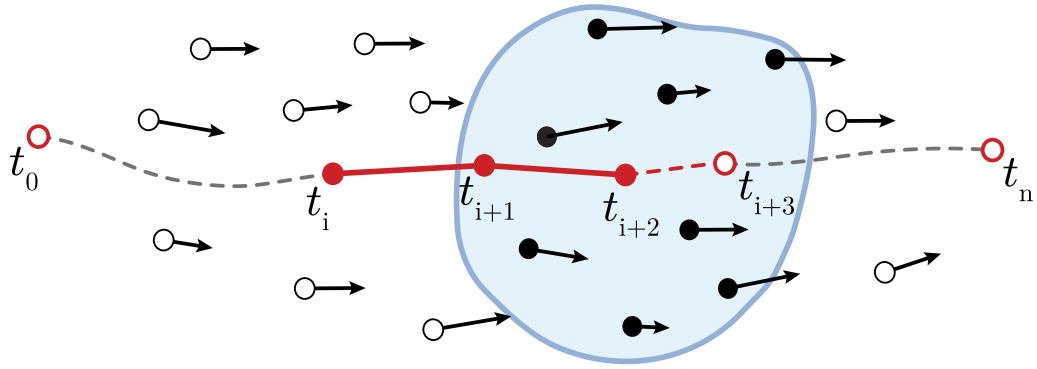

Figure 5. A pathline (solid red line) is drawn connecting the tracked positions of a particle from t_i to t_{i+2}. In order to extend the particle track forward, beyond its original length, to t_{i+3} the displacement (represented by black arrows) of other particles measured over that time step are considered. The movement of the nearest 10% of all particles (black circles within the blue area) are used to predict the displacement of the tracer in question. Forward extension continues in this fashion until the particle leaves the domain (t_n), whereas backward-time extension traces the particle back to its source (t_0).

frame to the next. The image enhancement methods described were sufficient to effectively track microbubbles downstream of the stenosis model.

2.6. Echo-Lagrangian particle tracking

Path-dependent dynamics are extracted from the preprocessed images using echoLPT following three steps: particle detection, particle tracking and path extension. Particle detection, using LaVision DaVis 8.4, is performed via peak thresholding, based on a case-specific intensity threshold and particle fit mode, that accurately returns the position of microbubbles detected at each time step. An 11 × 11 pixel Gaussian fit is employed to identify the relatively large particle images (up to 15 pixels wide away from the focus) captured using an ultrasound contrast agent. Despite the distorted shape of some of the particles, applying a Gaussian fit did not affect the ability to track said particle images. Figure 4(c) shows an overlay of the detected particles (red) on the filtered image. Detected particles are tracked from frame to frame using a peak-matching algorithm that searches within an allowable displacement range and maximum relative acceleration. The range is flow-specific and, because it is applied across the entire domain, can lead to erroneous matches for large dynamic ranges, e.g. a particle within the low-velocity recirculation region behind the stenosis may be assigned a non-physical velocity that is more appropriate for jet flow. Each particle's displacement is verified by checking the spatial coherence of particle velocities in its vicinity. Particles that find a valid match from one time step to the next are connected to form tracks. The pathlines produced are short, as is typical of optical LPT, so they must be extended to extract their full trajectory. Path extension follows the method described and implemented in Rosi and Rival (2018) and Jeronimo *et al* (2019a). Microbubble trajectories are traced backwards and forwards based on flow maps fit to the raw scattered echoLPT data at each time step using a locally-weighted regression (or LOWESS) algorithm. A flow map is a surface fitting function that considers the displacement of physical particle images, both forward and backward in time, and the nearest 10% of the detected particles to each, to extend the particle's motion past their tracked pathline. 10% of the neighbouring particle images corresponds to approximately 20 particles for these ultrasound images. For reference, an optical setup, capable of greater particle image density, may only require 1% of neighbouring particles to reach the same number. In figure 5 a track is extended forwards from t_{i+2} to t_{i+3} using a flow map fit based on the measured displacement of microbubbles within the blue area. While particle ambiguity limits the seeding density for echoLPT, flow map compilation requires a minimum microbubble concentration—too low and the flow maps may predict strong, non-physical velocity gradients. Forwards- and backwards-time flow maps are used to extend each track to its terminal position and back to its source. A unique track for each detected microbubble contains time-resolved positional data. After extending the particle tracks they are filtered a final time: if any single step is greater than the original allowable displacement range then the entire track is removed.

2.7. EchoLPT validation

Validation of the ultrasound setup and echoLPT was performed by comparing the measurement of a steady, straight pipe flow to results using UIV and a theoretical Hagen–Poiseuille profile. Figure 6 shows an example of the B-mode images used for this comparison (note the microbbuble concentration is increased for UIV) and the three profiles calculated using UIV, echoLPT and theory. The mean velocity profile plotted with UIV was done using a sliding sum-of-correlation algorithm and 24 × 24 pixel interrogation windows with 75% overlap. The Lagrangian information generated using echoLPT was interpolated on to an Eulerian grid and averaged across the width of the domain to give a profile that closely matches the theoretical result. The computed velocities are scan corrected, as described by Poelma (2017). While figure 6(b) demonstrates that Eulerian data is accessible from Lagrangian tracks, the following section will focus on and highlight the Lagrangian quantities that can be extracted using echoLPT, which are otherwise unobtainable with existing ultrasound techniques.

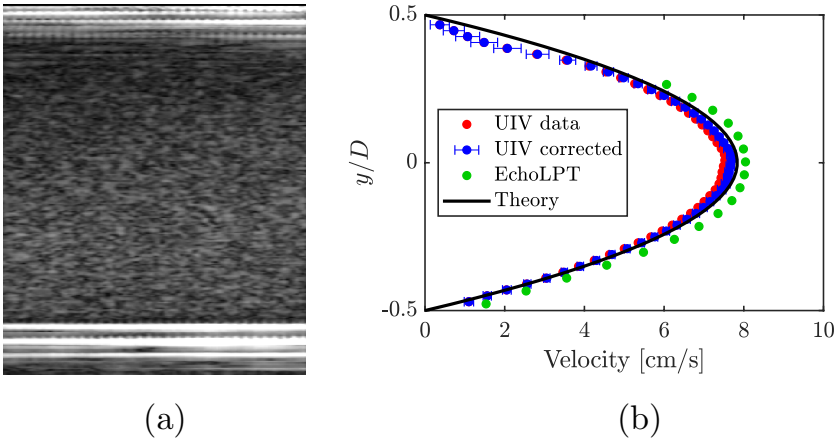

Figure 6. (a) Example of a raw image used for validation. The particle image density is made higher for use with UIV. (b) EchoLPT data is interpolated onto an Eulerian grid and the average velocity profile for steady flow through a straight pipe is compared to UIV results and the theoretical, Hagen–Poiseuille solution. The ability to match this profile verify the quality of the ultrasound-based measurements in this study.

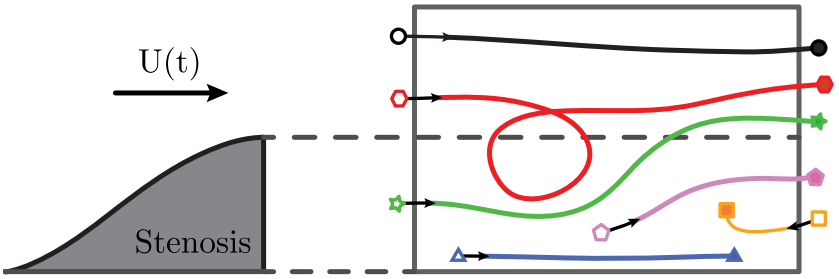

Figure 7. Tracked microbubbles are categorized based on their trajectory through the measurement domain and coloured accordingly. Jet particles (black) move quickly through the domain, while red and green particles mix with the fluctuations of the pulsatile flow. Blue particles remain within view throughout the motion, pink fluid is flushed out, and orange particles account for small amounts of retrograde flow.

3. Results

To demonstrate the value of the echoLPT technique, this section describes the flow in a post-stenotic region qualitatively, and quantitatively using PRT. First, microbubbles are categorized based on the extended trajectory they plot through the measurement domain in section 3.1. The pathlines reveal mixing in the recirculation region downstream of the stenosis and the generation of a vortical structure with each pulse of the flow rate. In section 3.2, the PRT of individual microbubbles is calculated and used to highlight differences in various pulsatile flow.

3.1. Post-stenotic flow behaviour

Over a recording period of five seconds (865 frames) an average of 50 000 unique microbubbles were tracked for each combination of flow parameters tested. The mean track length of those tracers was extended from only 4 frames to approximately 210 frames. Path extension allowed each physical particle track to exist in frames they were not originally detected in, which is equivalent to synthetically increasing the detected particle image density to 0.15 ppp. Qualitative information is obtained from the extended particle trajectories by colour-labelling particle images based on their source and terminal positions (see figure 7). Microbubbles that enter the measurement domain above the edge of the stenosis ($y/D > -0.25$) are coloured black or red, where red particles mix into the recirculation region and black ones do not. Blue particles remain within the domain throughout the recording, while pink particles are flushed out by green particles entering from upstream ($y/D \leqslant -0.25$). Small volumes of fluid recirculating into the measurement domain from downstream are labelled orange.

Figure 8 shows the motion of microbubble flow tracers downstream of the stenosis model, at $\alpha = 15$ and $\lambda = 1.0$, compared for each of the mean Reynolds numbers tested. The figure shows a single period of the pulsatile flow, beginning from the second pulse ($\phi = 2\pi$) of the recording. Particle tracking reveals distinct differences in the behaviour of the flow at $\mathrm{Re}_m = 32$ compared to the other two: Large volumes of blue and pink particles remain within the domain throughout the pulse and there is very little mixing of the red and green particles. At $\mathrm{Re}_m = 64$ the net flow close to the wall is still small, but the formation of a large vortex ring at the beginning of each pulse ($\phi = 2\pi$ and 4π) is observed. The vortical structure (previously reported for pulsatile stenotic flows by Sherwin and Blackburn (2005) and Varghese *et al* (2007)) sweeps red particles down into the recirculation region and then convects downstream. The periodic motion of the recirculation region and the vortex ring at $\mathrm{Re}_m = 64$ can be seen in

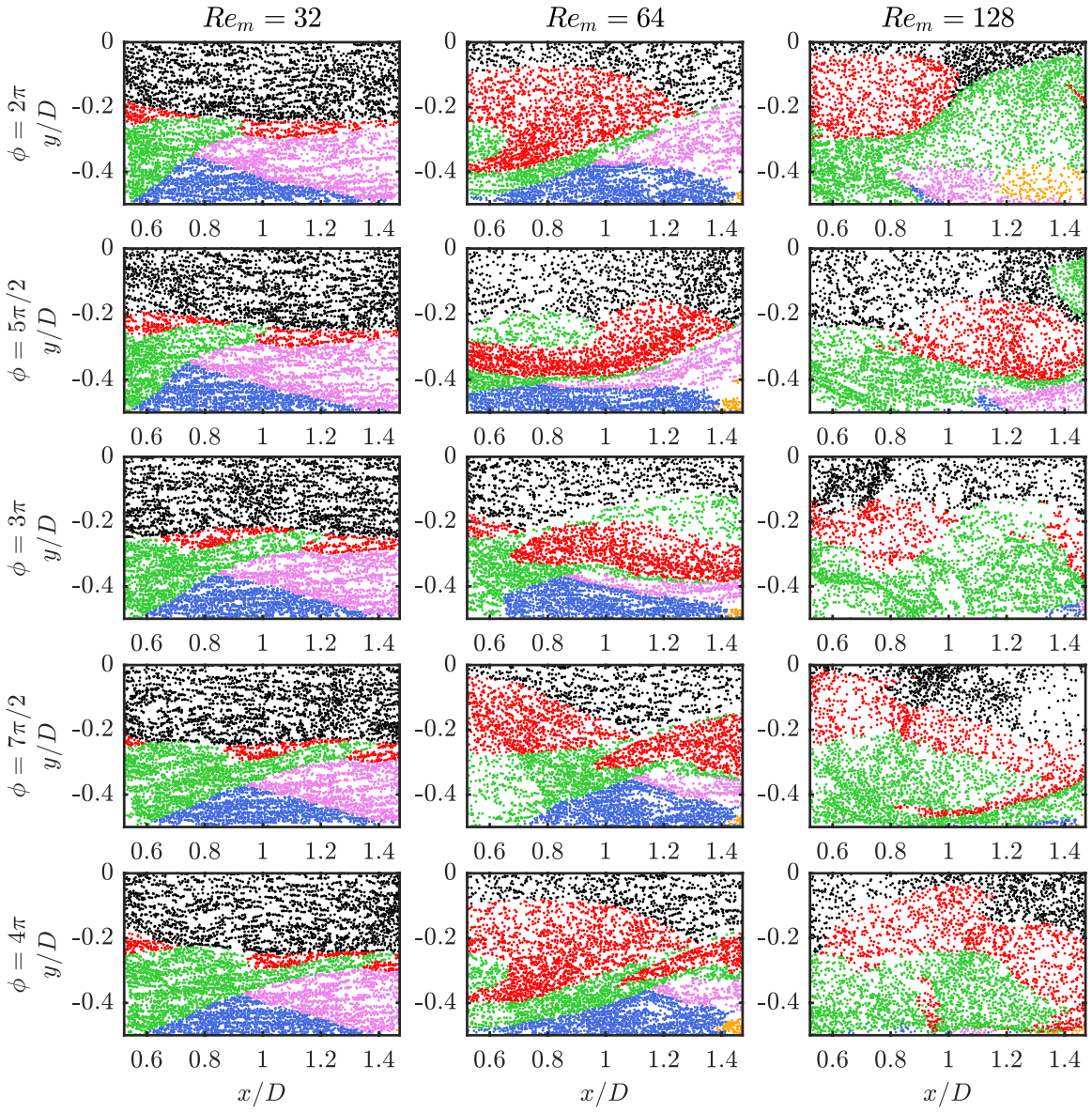

Figure 8. Flow through a stenosis model is tracked using echoLPT. Individual particle trajectories are mapped and labelled according to their trajectory through the measurement domain following the method described by Jeronimo *et al* (2019a). Pulsatile flow at each of the Re_m tested is compared for $\alpha = 15$ and $\lambda = 1.0$.

Video 3 over five periods. For $\mathrm{Re}_m = 128$, most of the initial fluid has already been flushed from view after a single pulse and it appears the vortex roll-up is shifted further downstream and not fully captured in the transducer's narrow field of view.

3.2. Measuring PRT

EchoLPT allows information to be extracted from every microbubble that passes through the stenosis geometry along the time-resolved pathlines depicted in figure 8. The value of the echoLPT technique is demonstrated by calculating the PRT along each pathline. PRT is a path-dependent quantity defined as the length of time a fluid parcel remains within a region of interest, normalized by the period of the pulsatile flow, and relates directly to the length of the pathlines drawn in the post-stenotic measurement domain. The growth of microbubble PRT in the recirculation region over a single pulse ($2\pi \leq \phi \leq 4\pi$) is shown in figure 9 for each of the Re_m investigated. The time-resolved PRT of the fluid over a series of pulses can be observed in Video 3 for $\mathrm{Re}_m = 64$, $\alpha = 15$ and $\lambda = 1.0$. When animated, the motion of some particles experience jitter. The jitter is the result of changes to the particle image shape from frame-to-frame that shifts the position of the particle's peak intensity. Fortunately, the resultant displacements are small and have no significant effect on path length or PRT calculations. The results in this section were measured for the entire measurement domain, as indicated in figure 2(b), however, PRT can be calculated for any subset of the domain, i.e. to compare PRT within the jet versus the near-wall region (figure 10). The mean PRT for particles that entered one of the three demarcated regions in figure 10 are 0.13 (top), 0.88 (bottom-left) and 1.20 (bottom-right), over five periods ($\phi = 10\pi$) at $\mathrm{Re}_m = 64$, $\alpha = 15$ and $\lambda = 1.0$.

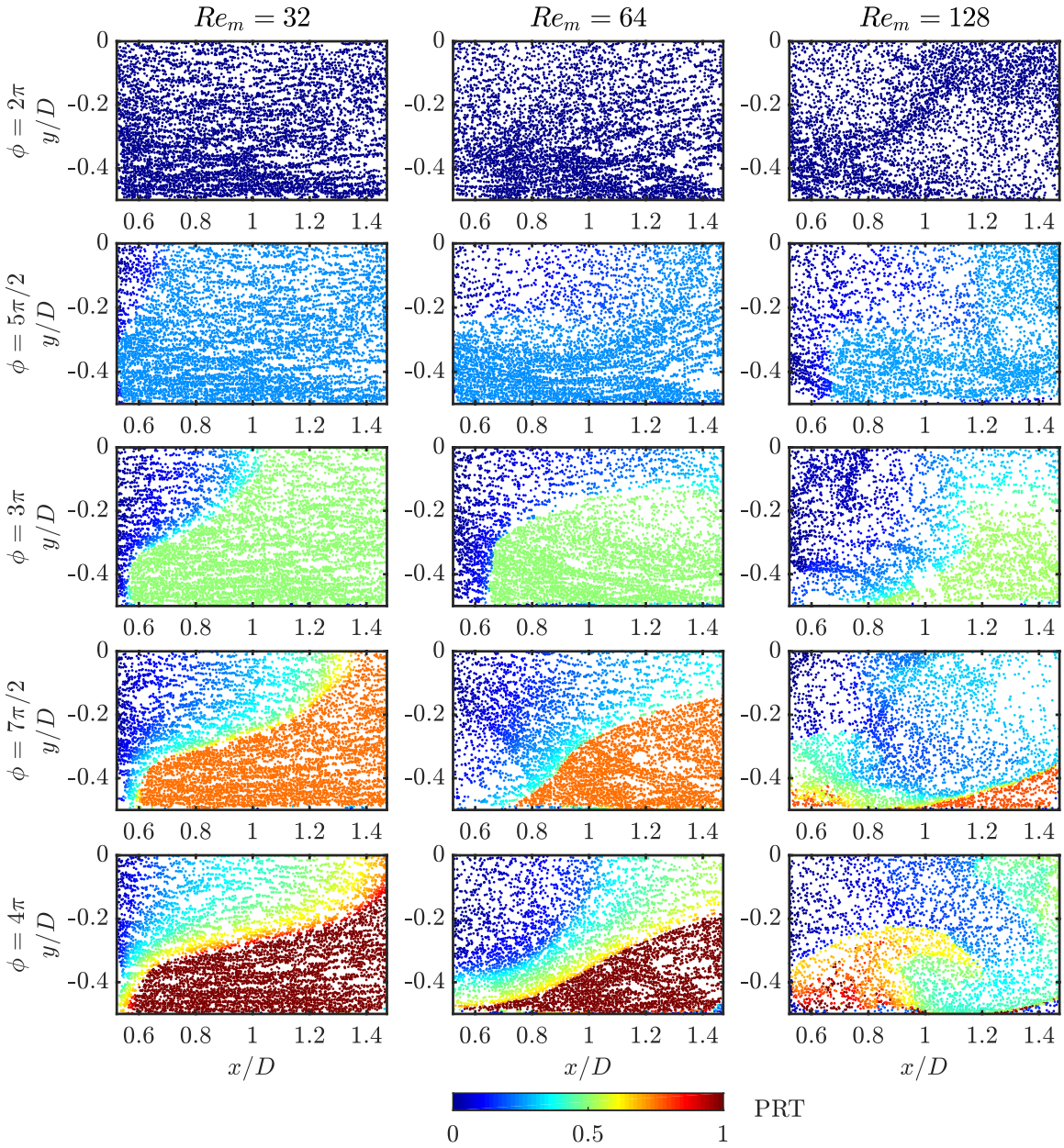

Figure 9. PRT is extracted from a post-stenotic flow using echoLPT by mapping the trajectory of each particle that enters the measurement domain. The tracked microbubbles are coloured according to their instantaneous PRT over the course of a single pulse. These results are for a pulsatile flow with $\alpha = 15$ and $\lambda = 1.0$ at each Re_m tested.

The effect pulsatility has on post-stenotic flow is evaluated by plotting the probability distribution (PDF) of the total PRT of select fluid parcels. Specifically, the impact of Re_m, α and λ are judged by only comparing the PRT of particles that were labelled red (in figure 8) and pass through the measurement domain during the recording, i.e. the PRT was not shortened by the beginning or end of the recording. Figure 11(a) is the PDF of the PRT of red particles compared for each Re_m at $\alpha = 15$ and $\lambda = 1.0$. The mean PRT decreases with increasing Re_m for every combination of flow conditions tested, as is expected of flows with a higher mean velocity. The shape of the PDF, however, is indicative of the flow behaviour seen in figure 8: (i) at $\mathrm{Re}_m = 32$, there is little to no mixing and PRT fall within a narrow range; (ii) at $\mathrm{Re}_m = 64$, vortex growth affects some red particles more than others and spreads the PRT distribution; and (iii) at $\mathrm{Re}_m = 128$, the narrow band of PRT is the result of only a portion of the vortical structure being captured within the measurement domain. The effects of increasing the frequency and amplitude are highlighted by observing the PRT of pulsatile flow at $\mathrm{Re}_m = 64$, as seen in figure 11(b). The mean PRT is prolonged at higher α, and microbubbles that are mixed into the recirculation region remain within the domain for more than a single pulse. The generation of a vortex ring with each pulse sweeps particles from the jet down and backwards, and delays their traversal of the domain. Increasing λ causes a small decrease in the mean PRT at each value of α. The larger velocity gradient quickly propels fluid through the domain and limits mixing; this effect is stronger at higher α.

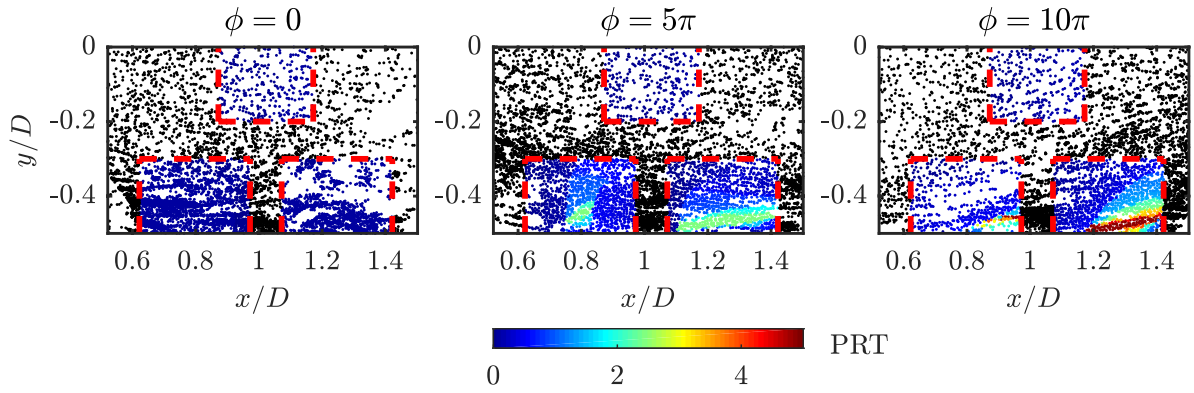

Figure 10. PRT can be calculated for any subset of the measurement domain. Here the instantaneous PRT is plotted for particles entering three subregions, outlined in red, over the course of five pulses. At $\mathrm{Re}_m = 64$, $\alpha = 15$ and $\lambda = 1.0$, the mean PRT in each of the regions is 0.13 (top), 0.88 (bottom-left) and 1.20 (bottom-right).

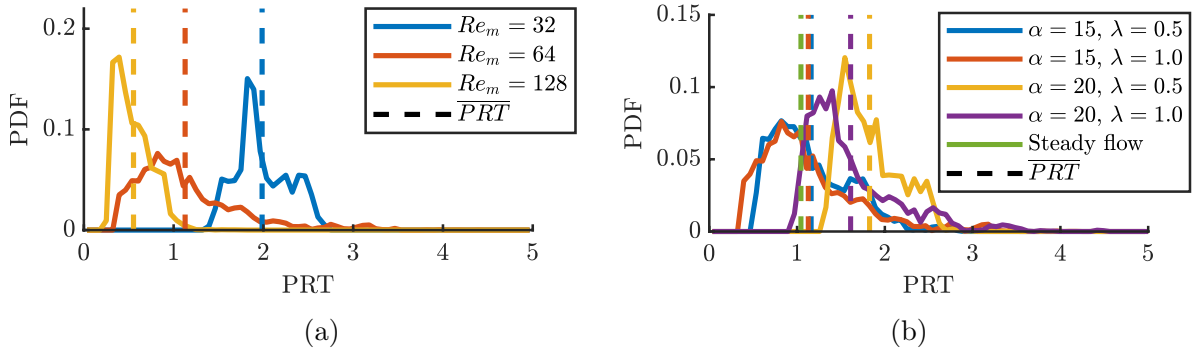

Figure 11. The PRT of pulsatile flows is compared by plotting the probability density function of the PRT of red-labelled particles that pass through the measurement domain: (a) PRT decreases with increasing Re_m at $\alpha = 15$ and $\lambda = 1.0$; and (b) α increases PRT, while λ decreases mean PRT at $\mathrm{Re}_m = 64$. For all cases the PRT of pulsatile flow is increased compared to steady flow at the same Re_m. Dashed lines represent the mean PRT ($\overline{PRT}$) of each flow.

The value of echoLPT is clearly demonstrated by measuring the effects of pulsatility on PRT for flow at $\mathrm{Re}_m = 64$.

4. Conclusions

After years of development, optical PIV and LPT techniques are now well-established tools for the study of complex fluid physics. The introduction of UIV provided a means of performing Eulerian field measurements in opaque and *in vivo* flows, but there is still no approach for the extraction of Lagrangian metrics using ultrasound images. In the current study, the feasibility of ultrasound-based particle tracking is demonstrated using a novel method, named echo-Lagrangian particle tracking, of measuring path-dependent dynamics. Optimization of echoLPT, including imaging parameters, material choices and seeding particles, is discussed in detail. The technique is showcased by tracking the behaviour of pulsatile flows through an idealized stenosis geometry and comparing the time-resolved PRT of individual fluid parcels.

Ultrasound images have a characteristically low signal-to-noise ratio and the recording process must be tailored for particle tracking. The acoustic power and seeding particles, and their concentration, were each chosen to minimize surface reflections and particle ambiguity, while ultrasound parameters, including line density and scan depth, were adjusted to maximize frame rate. Particle detection and tracking require that B-mode images are preprocessed to amplify the signal-to-noise ratio. Background, smoothing, and sharpening filters assist in isolating microbubbles that can be tracked and extended to map their entire trajectory. EchoLPT was capable of tracking thousands of unique flow tracers as they exited a stenosis. The ability to monitor particle-specific characteristics, like PRT, is of great value to the medical community. PRT was measured for each microbubble that entered the region of interest and elucidates differences in pulsatile flow behaviour for increasing Re_m, α and λ. As a means of demonstrating the value of the current approach, it was shown that higher values of α encouraged mixing into the near-wall region and prolonged PRT, while large velocity gradients increased particle turnover and decreased PRT.

The current echoLPT technique remains grounded by the limitations and quality of ultrasound imaging. The field of view, depth of scan, dynamic range and streamwise resolution all limit the frame rate. As a result, the flows tested were restricted to low Reynolds numbers and amplitude ratios. Fluctuating particle image shape and strong surface reflections each affect the ability to detect and track tracer particles over long distances. While acquisition rates and image quality will inevitably improve with advancements of the underlying ultrasound technology (plane-wave imaging has potential for high-frame rate ultrasound, Rodriguez *et al* (2013) and

Leow *et al* (2015)), future studies will attempt to account for irregular (non-Gaussian) particle image shape, using a custom detection algorithm, and incorporate existing UIV techniques to improve particle matching.

Acknowledgments

MDJ acknowledges the support of the Natural Sciences and Engineering Research Council of Canada (NSERC) Alexander Graham Bell Canada Graduate Scholarship (CGS-D) and DER wishes to thank the NSERC Discovery Grant for supporting this research.

ORCID iDs

M D Jeronimo https://orcid.org/0000-0002-0391-273X
M R Najjari https://orcid.org/0000-0002-0898-6287
D E Rival https://orcid.org/0000-0001-7561-6211

References

Ackermann D and Schmitz G 2016 Detection and tracking of multiple microbubbles in ultrasound b-mode images *IEEE Trans. Ultrason. Ferroelectr. Freq. Control* **63** 72–82
Adrian R J and Westerweel J 2011 *Particle Image Velocimetry* (Cambridge: Cambridge University Press)
Contreras Ortiz S H, Chiu T and Fox M D 2012 Ultrasound image enhancement: a review *Biomed. Signal Process. Control* **7** 419–28
Crapper M, Bruce T and Gouble C 2000 Flow field visualization of sediment-laden flow using ultrasonic imaging *Dyn. Atmos. Oceans* **31** 233–45
Elkins C J and Alley M T 2007 Magnetic resonance velocimetry: applications of magnetic resonance imaging in the measurement of fluid motion *Exp. Fluids* **43** 823–58
Gallot T, Perge C, Grenard V, Fardin M A, Taberlet N and Manneville S 2013 Ultrafast ultrasonic imaging coupled to rheometry: principle and illustration *Rev. Sci. Instrum.* **84** 045107
Gurung A and Poelma C 2016 Measurement of turbulence statistics in single-phase and two-phase flows using ultrasound imaging velocimetry *Exp. Fluids* **57** 171
Hong G R *et al* 2008 Characterization and quantification of vortex flow in the human left ventricle by contrast echocardiography using vector particle image velocimetry *JACC: Cardiovascular Imaging* **1** 705–17
Im K S, Fezzaa K, Wang Y J, Liu X, Wang J and Lai M C 2007 Particle tracking velocimetry using fast x-ray phase-contrast imaging *Appl. Phys. Lett.* **90** 091919
Jensen J A, Nikolov S I, Yu A C H and Garcia D 2016b Ultrasound vector flow imaging—part II: parallel systems *IEEE Trans. Ultrason. Ferroelectr. Freq. Control* **63** 1722–32
Jensen J A, Nikolov S, Yu A C and Garcia D 2016a Ultrasound vector flow imaging: I: sequential systems *IEEE Trans. Ultrason. Ferroelectr. Freq. Control* **63** 1704–21
Jeronimo M D, Najjari M R, Zhang K and Rival D E 2019b Extraction of particle residence time using echo-Lagrangian particle tracking *13th Int. Symp. on Particle Image Velocimetry (Munich, Germany)* (https://athene-forschung.unibw.de/128884)
Jeronimo M D, Zhang K and Rival D E 2019a Direct Lagrangian measurements of particle residence time *Exp. Fluids* **60** 72
Kertzscher U, Seeger A, Affeld K, Goubergrits L and Wellnhofer E 2004 X-ray based particle tracking velocimetry-a measurement technique for multi-phase flows and flows without optical access *Flow Meas. Instrum.* **15** 199–206
Kheradvar A, Houle H, Pedrizzetti G, Tonti G, Belcik T, Ashraf M, Lindner J R, Gharib M and Sahn D 2010 Echocardiographic particle image velocimetry: a novel technique for quantification of left ventricular blood vorticity pattern *J. Am. Soc. Echocardiography* **23** 86–94
Kim H B, Hertzberg J R and Shandas R 2004 Development and validation of echo PIV *Exp. Fluids* **36** 455–62
La Porta A, Voth G A, Crawford A M, Alexander J and Bodenschatz E 2001 Fluid particle accelerations in fully developed turbulence *Nature* **409** 1017–9
Lee S J and Kim S 2005 Simultaneous measurement of size and velocity of microbubbles moving in an opaque tube using an x-ray particle tracking velocimetry technique *Exp. Fluids* **39** 492–7
Leow C H and Tang M X 2018 Spatio-temporal flow and wall shear stress mapping based on incoherent ensemble-correlation of ultrafast contrast enhanced ultrasound images *Ultrasound Med. Biol.* **44** 134–52
Leow C H, Bazigou E, Eckersley R J, Yu A C, Weinberg P D and Tang M X 2015 Flow velocity mapping using contrast enhanced high-frame-rate plane wave ultrasound and image tracking: methods and initial *in vitro* and *in vivo* evaluation *Ultrasound Med. Biol.* **41** 2913–25
Niu L, Qian M, Yan L, Yu W, Jiang B, Jin Q, Wang Y, Shandas R, Liu X and Zheng H 2011 Real-time texture analysis for identifying optimum microbubble concentration in 2D ultrasonic particle image velocimetry *Ultrasound Med. Biol.* **37** 1280–91
Poelma C 2017 Ultrasound imaging velocimetry: a review *Exp. Fluids* **58** 3
Raffel M, Willert C E, Scarano F, Käehler C J, Wereley S T and Kompenhans J 2018 *Particle Image Velocimetry: a Practical Guide* 2nd edn (New York: Springer) (https://doi.org/10.1007/978-3-319-68852-7)
Rodriguez S, Jacob X and Gibiat V 2013 Plane wave echo particle image velocimetry *Proc. Meetings on Acoustics* **19** 030116
Rosi G A and Rival D E 2018 A Lagrangian perspective towards studying entrainment *Exp. Fluids* **59** 19
Sampath K, Harfi T T, George R T and Katz J 2018 Optimized time-resolved echo particle image velocimetry-particle tracking velocimetry measurements elucidate blood flow in patients with left ventricular thrombus *J. Biomech. Eng.* **140** 041010
Sherwin S J and Blackburn H M 2005 Three-dimensional instabilities and transition of steady and pulsatile axisymmetric stenotic flows *J. Fluid Mech.* **533** 297–327
Song P, Trzasko J D, Manduca A, Huang R, Kadirvel R, Kallmes D F and Chen S 2018 Improved super-resolution ultrasound microvessel imaging with spatiotemporal nonlocal means filtering and bipartite graph-based microbubble tracking *IEEE Trans. Ultrason. Ferroelectr. Freq. Control* **65** 149–67
Tambasco M and Steinman D A 2003 Path-dependent hemodynamics of the stenosed carotid bifurcation *Ann. Biomed. Eng.* **31** 1054–65
van Ooij P, Guédon A, Poelma C, Schneiders J, Rutten M C M, Marquering H A, Majoie C B, vanBavel E and Nederveen A J 2011 Complex flow patterns in a real-size intracranial aneurysm phantom: phase contrast MRI compared with particle image velocimetry and computational fluid dynamics *NMR Biomed.* **25** 14–26
Varghese S S, Frankel S H and Fischer P F 2007 Direct numerical simulation of stenotic flows. Part 2. Pulsatile flow *J. Fluid Mech.* **582** 281–318
Walker A M, Scott J, Rival D E and Johnston C R 2014 *In vitro* post-stenotic flow quantification and validation using echo particle image velocimetry (Echo PIV) *Exp. Fluids* **55** 1821
Zhang F *et al* 2011 *In vitro* and preliminary *in vivo* validation of echo particle image velocimetry in carotid vascular imaging *Ultrasound Med. Biol.* **37** 450–64